Spin-mass vortex in ^{3}He-B: Order-parameter texture and NMR signature

J. Kopu and M. Krusius
Low Temperature Laboratory, Helsinki University of Technology, 02150 Espoo, Finland
(Received 22 February 2001; published 3 August 2001)

We have calculated numerically the change in the NMR signal of rotating superfluid ^{3}He-B induced by the presence of one spin-mass vortex. The NMR line shape is determined from the equilibrium distribution of the order-parameter axis $\hat{\mathbf{n}}(\mathbf{r})$. Depending on the external conditions, two textures of different symmetry and with clearly distinguishable NMR behavior are obtained. One of these agrees with published NMR measurements; the other has not been reported earlier. The methods are discussed by which the texture transition and the new reflection-symmetric texture could be observed experimentally.

DOI: 10.1103/PhysRevB.64.094504 PACS number(s): 67.57.Fg

The broken symmetries and the structure of the order parameter in superfluid ^{3}He are manifest in the existence of several stable topological defects with different dimensionalities. One of the most extraordinary examples is the combination of a spin-mass vortex (SMV) and a soliton sheet in the B phase. This composite object was discovered in measurements where a container rotating at constant angular velocity was slowly cooled from ^{3}He-A to ^{3}He-B.[1,2] Its identification was partly based on earlier theoretical work[3] which had suggested its existence. More recent measurements have demonstrated that it is also created within bulk ^{3}He-B liquid in the presence of ionizing radiation and vortex-free counterflow at sufficiently high velocity.[4] In contrast, it is normally not created when the counterflow velocity at the wall of the rotating container reaches the critical value for vortex formation.[5]

The presence of the spin-mass vortex leads to changes in the NMR spectrum when it is measured at low rf excitation in a polarizing magnetic field which is oriented parallel to the rotation axis. These changes are small and can be easily lost in the measuring noise. The present numerical calculations of B-phase order-parameter textures, which incorporate a spin-mass vortex, are intended to provide a better understanding of what to look for in future measurements. Our results show that the identification of the SMV ''fingerprint,'' which was used to analyze the measurements of Ref. 4, is quantitatively correct. However, the calculations also indicate that interesting effects can be expected if the SMV textures are investigated as a function of the vortex-free counterflow velocity.

Spin-mass vortex. The degenerate equilibrium states of ^{3}He-B are labeled by a phase Φ and a rotation matrix $\vec{R}(\hat{\mathbf{n}},\theta)$. Two different types of linear defects exist in these variables: an ordinary vortex with circulating mass flow and a disclination (or a spin vortex) with spin current around it. Roughly speaking, while in a mass vortex the phase Φ changes by 2π, in a disclination the rotation angle θ changes by 2π with the rotation axis $\hat{\mathbf{n}}$ (of unit length) kept constant. Since both a mass vortex and a spin vortex have a hard core (of the size of the superfluid coherence length ξ) where the superfluid state is strongly deformed, it is energetically advantageous for a pair to form a common core.[3] The resulting object is called a SMV.

Far from the core, the large-scale structure of a disclination is determined by the dipolar spin-orbit interaction, which tends to fix θ equal to $\theta_0=\arccos(-1/4)\approx 104°$. This value is assumed by most of the liquid surrounding the SMV. However, for topological reasons the disclination is necessarily accompanied by a planar defect, a θ soliton, where θ changes from θ_0 to 180° and back, but with opposite direction of $\hat{\mathbf{n}}$.[6] The gradient energy $F_G=\int d^3\mathbf{r}[\lambda_{G1}\partial_i R_{\alpha i}\partial_j R_{\alpha j}+\lambda_{G2}\partial_i R_{\alpha j}\partial_i R_{\alpha j}]$ is minimized when $\hat{\mathbf{n}}$ is perpendicular to the plane of the soliton because then the λ_{G1} term gives no contribution. The order-parameter variation inside the soliton has been calculated in Ref. 7. Since the dipole energy is not minimized within the soliton, its size is determined by the corresponding healing length, the dipole length $\xi_D\approx 10\ \mu$m. Outside the soliton only $\hat{\mathbf{n}}$ changes with position.

The soliton tail of the SMV can either bind two SMV's together or terminate at the container wall. Here we concentrate on the latter possibility, which is presented in Fig. 1. In the presence of vortex-free counterflow of the normal and superfluid components with velocities $\mathbf{v}=\mathbf{v}_n-\mathbf{v}_s$, the surface tension of the soliton is balanced by the Magnus force on the mass vortex, which prevents the object from shrinking. The composite structure can therefore be stabilized in experiments in a rotating container and identified on the basis of its NMR signature.[1,2,4]

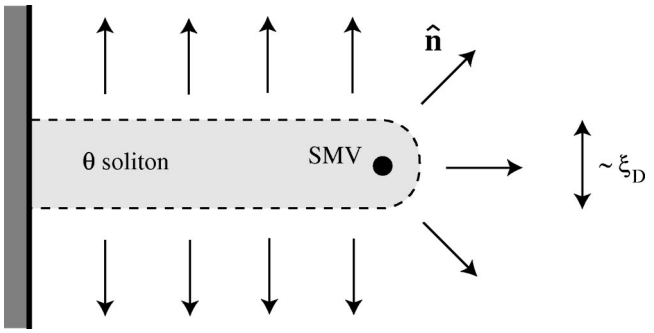

FIG. 1. Schematic representation of the spin-mass vortex (black dot) with a domain-wall-like soliton tail (gray area surrounded by the dashed line) ending at the container wall. The thickness of the soliton is of the order of the dipole length ξ_D. Outside the soliton $\theta=\theta_0$ and the direction of $\hat{\mathbf{n}}$ changes as indicated by the arrows. On crossing the soliton, θ changes from θ_0 to 180° and back, with reversed $\hat{\mathbf{n}}$ [note that the rotations given by $(\hat{\mathbf{n}},180°)$ and $(-\hat{\mathbf{n}},180°)$ are equivalent].

NMR of $\hat{\mathbf{n}}$ *textures*. Our goal is to calculate the *B*-phase order-parameter texture and the corresponding NMR absorption signal in situations which closely relate to planned measurements. The calculation is intended to provide guidelines on how to identify the presence of the SMV from the measured NMR spectra and what new features one might expect. We concentrate on the conventional NMR response, with the rf excitation field oriented perpendicular to the polarizing field. The rf excitation is continuously applied in the low-amplitude limit, so that the precession angle remains small and no unconventional coherent *B*-phase resonance modes are excited.

If the local variation of the *B*-phase anisotropy axis $\hat{\mathbf{n}}$ extends over a length scale which is long compared to the dipolar healing length ξ_{D}, then the general line shape of the NMR absorption signal can be obtained from the spatial distribution of the $\hat{\mathbf{n}}$ orientation. If moreover the polarizing field $\mathbf{H}$ is oriented parallel to the symmetry axis $\hat{\mathbf{z}}$ of the cylindrical container and the *B*-phase textural magnetic healing length ξ_{H} is small compared to the radius R of the cylinder, then the highly symmetric $\hat{\mathbf{n}}$ textures of ''flare-out'' form are created.[8]

The first step in our calculations is to find out how the flare-out texture is distorted in the presence of a SMV. The second step is to calculate the changes in the NMR line shape. The latter is done using the local oscillator model where the local frequency shift, measured from the Larmor frequency, is determined by the local orientation of $\hat{\mathbf{n}}$ with respect to the polarizing field $\mathbf{H}$. Thus the NMR line shape of absorption versus frequency shift is used to provide an image of the $\hat{\mathbf{n}}$ texture.

It has been known since the measurements by Osheroff[9] that even at low-rf-excitation-level collective resonances, trapped spin-wave modes can be excited. In the NMR spectrum (with absorption plotted versus frequency shift), these are observed as periodic oscillations in the absorption level, superimposed on the general texture-dependent line shape. In the flare-out texture they have been extensively studied and used as a measuring tool for vortex lines.[10] They exist close to the Larmor frequency, which spatially means the region close to the cylindrical symmetry axis, where the polar angle β of the $\hat{\mathbf{n}}$ orientation slowly starts to open up from the external field $\mathbf{H}$ direction. The small linear gradient in $\beta(r)$ provides the confining potential for trapping the spin-wave resonances. In the presence of a SMV and the confining vortex-free counterflow, which is needed for its stabilization, the $\hat{\mathbf{n}}(\mathbf{r})$ texture is more inhomogeneous and the shallow gradient of $\beta(r)$ in the center of the vortex cluster is destroyed. In this situation spin-wave resonance excitations are not expected to be prominent and have so far not been experimentally observed. In the present calculation we shall neglect them.

Theoretical model. For our calculations we use the method described in Ref. 11. The procedure starts with determining the equilibrium distribution of $\hat{\mathbf{n}}=(-\hat{\mathbf{r}}\cos\alpha+\hat{\boldsymbol{\phi}}\sin\alpha)\sin\beta+\hat{\mathbf{z}}\cos\beta$, where $\hat{\mathbf{r}}$, $\hat{\boldsymbol{\phi}}$ and $\hat{\mathbf{z}}$ are the unit vectors of the cylindrical coordinate system. This is done with the hydrostatic theory of ^{3}He-*B* (see Ref. 12 for a review and a full list of references). The main orienting interactions are due to the external magnetic field $\mathbf{H}\|\hat{\mathbf{z}}$, with energy $F_{\mathrm{DH}}=-a\int d^3\mathbf{r}(\hat{\mathbf{n}}\cdot\mathbf{H})^2$, counterflow $\mathbf{v}$ produced by rotating the cylinder, $F_{\mathrm{HV}}=-\lambda_{\mathrm{HV}}\int d^3\mathbf{r}(\mathbf{H}\cdot\vec{R}\cdot\mathbf{v})^2$, and the surfaces of the container, $F_{\mathrm{SH}}=-d\int d^2\mathbf{r}(\mathbf{H}\cdot\vec{R}\cdot\hat{\mathbf{r}})^2$. Here we restrict ourselves to the case of an infinitely long cylinder and ignore any dependence on the coordinate z.

We allow for metastable rotating states, with less than the equilibrium number of mass vortex lines, which are confined by the Magnus force into a central coaxial cluster of vortex lines. The flow velocity in the surrounding annular vortex-free counterflow region around a cluster of N_{V} vortex lines is $v=\Omega r-\kappa N_{\mathrm{V}}/(2\pi r)$, where $\kappa=0.0662$ mm^2/s is the quantum of circulation in ^{3}He. The distortion of the superfluid state within the cluster introduces an additional orienting energy term equal to $F_{\mathrm{LH}}=\lambda_{\mathrm{LH}}\int_L d^3\mathbf{r}(\mathbf{H}\cdot\vec{R}\cdot\hat{\mathbf{z}})^2$, where the integration is over the region occupied by the rectilinear vortex lines. The different orienting effects are in conflict with each other, leading to the formation of an inhomogeneous $\hat{\mathbf{n}}(\mathbf{r})$ texture in the cylinder. The bending of $\hat{\mathbf{n}}$ is opposed by the gradient energy F_{G}. The length scale of the resulting spatial variation is the magnetic healing length ξ_{H}, which is determined by equating F_{G} with the magnetic-field energy F_{DH}. Typically $\xi_{\mathrm{H}}\sim 0.1$–1 mm and it is inversely proportional to the magnetic-field strength H. Likewise, equating F_{DH} with F_{HV} defines the dipolar velocity v_{D} (~ 1 mm/s), which gauges the strength of the flow energy.

The top part of Fig. 2 represents the variation of $\hat{\mathbf{n}}$ in the flare-out configuration, where the angular variables defining $\hat{\mathbf{n}}$ only depend on the radial coordinate, $\alpha=\alpha(r)$, $\beta=\beta(r)$. In this case the texture problem is reduced to one spatial dimension. However, the presence of a single SMV in the cylinder breaks the rotational symmetry of the $\hat{\mathbf{n}}$ distribution (see the bottom part of Fig. 2). Therefore we have to consider in the texture calculation a more general situation with $\alpha=\alpha(r,\phi)$, $\beta=\beta(r,\phi)$. We calculate the texture on a two-dimensional lattice with N and M equidistant nodes in the radial and azimuthal directions, respectively ($N\Delta r=R, M\Delta\phi=2\pi$). The lattices used in the calculations have $N=20,\ldots,30$ and $M=75,\ldots,100$.

The frequency distribution due to the texture is given in the high-field limit by the approximate equation $\omega(\mathbf{r})\approx\omega_0+(\Omega_{\mathrm{B}}^2/2\omega_0)\sin^2\beta(\mathbf{r})$, where ω_0 is the Larmor frequency and Ω_{B} is the *B*-phase longitudinal resonance frequency. The main features of the line shape can be understood as follows: At low angular velocities Ω most of the absorption is accumulated close to ω_0 (apart from a small tail caused by the surface energy F_{SH}), because the magnetic-field energy F_{DH} is minimized by having $\beta=0$. On increasing the rotation velocity in the absence of vortex lines, the texture begins to orient towards $\sin^2\beta=0.8$ favored by the flow energy F_{HV}, leading to a gradual formation of another peak in the spectrum, the counterflow peak.

Modified flare-out state. Figure 2 shows the typical form of the equilibrium $\hat{\mathbf{n}}(\mathbf{r})$ texture, projected onto the plane perpendicular to the cylinder axis, without and with a SMV. We have fixed the position of the SMV to the edge of a cluster, which consists of N_{V} vortex lines, corresponding to the equi-

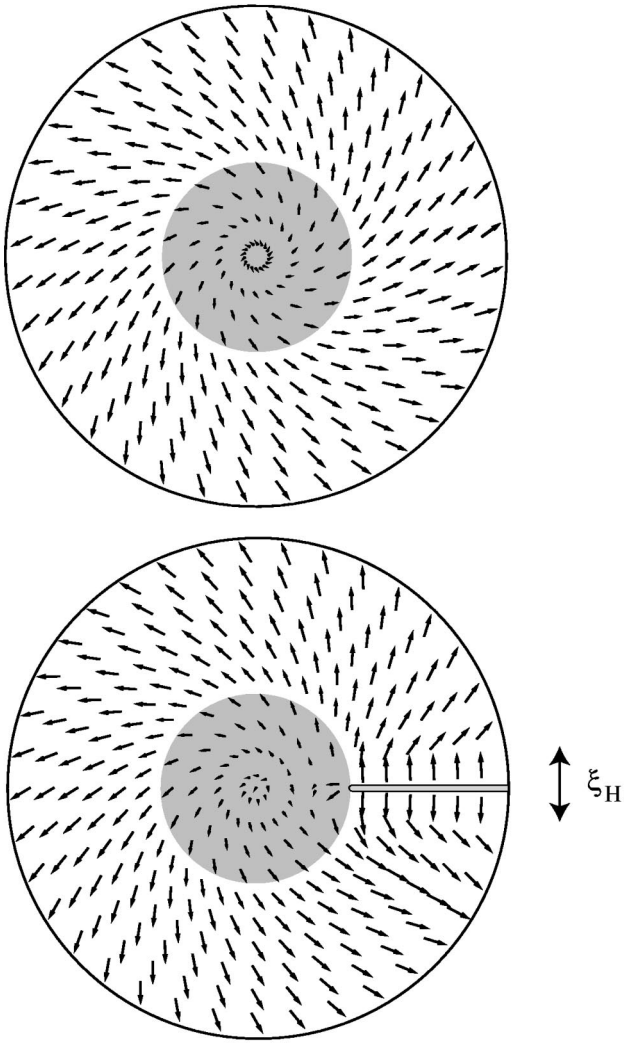

FIG. 2. Calculated equilibrium textures in a cylinder with $R=2.9$ mm, pressure $p=29.3$ bars, temperature $T=0.75\,T_c$ (T_c is the superfluid transition temperature), $H=20$ mT, $\Omega=2$ rad/s, and $N_V=320$ vortex lines. The arrows show the projection of $\hat{\mathbf{n}}$ in the plane perpendicular to the cylinder axis. The flare-out texture is shown on the top, and the modified texture due to the presence of a SMV and its soliton tail on the bottom. The shaded area denotes the vortex cluster.

librium number at the angular velocity $\Omega_V<\Omega$.[13] This assumption is well justified, since it can be shown that the surface tension of the soliton tail imposes only a small correction to the equilibrium position of the SMV.[1] Because of the small thickness $\sim\xi_D\ll\xi_H$ of the soliton wall, its effect must be treated as a boundary condition for the texture. In our calculations, we fixed the direction of $\hat{\mathbf{n}}$ to $\hat{\phi}$ and $-\hat{\phi}$ at adjacent lattice sites around the soliton. As already noted, this choice minimizes the gradient energy contribution, which dominates over the other weaker orienting interactions.

From Fig. 2 it is possible to understand qualitatively the change in the NMR line shape induced by the presence of the defect. The soliton wall forces $\hat{\mathbf{n}}$ to the plane perpendicular to the cylinder axis, which corresponds to having $\sin^2\beta=1$.

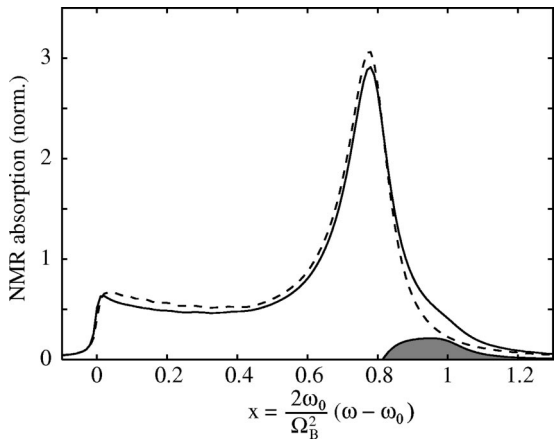

FIG. 3. Calculated normalized NMR spectra for the textures in Fig. 2. The dashed line corresponds to the flare-out texture and the solid line to the case with the SMV. The integrated total absorptions of both spectra are equal. The shaded area denotes the extra absorption due to the soliton, obtained by subtracting the two spectra from each other at $x\geqslant 0.8$. Experimentally this has been the ''fingerprint'' signal (Refs. 2 and 4) from which the presence of the SMV has been inferred. In the above spectra the additional line broadening is described by two parameters: the average magnetic-field inhomogeneity $\Delta H/H=3.4\times10^{-4}$ and the Leggett-Takagi relaxation time $\tau_{LT}=0.15\ \mu$s.

Therefore, some extra absorption accumulates in the interval $0.8<\sin^2\beta\leqslant 1$ due to the region close to the defect. The change in the calculated NMR absorption spectrum is illustrated in Fig. 3. To produce realistic line shapes, as close to the actual measured ones as possible, we have taken into account line broadening due to magnetic-field inhomogeneity and intrinsic Leggett-Takagi relaxation (for details see Ref. 11). We express the frequency in dimensionless units of $x\equiv(2\omega_0/\Omega_B^2)(\omega-\omega_0)$, and the NMR spectra are normalized so that the integrated area under the absorption curve equals unity.

Reflection-symmetric state. In addition to the modified flare-out texture in Fig. 2, a second texture of different symmetry was discovered. This texture is nearly symmetric under a reflection with respect to the plane of the soliton and is shown in Fig. 4. A transition to this texture can be induced by increasing the rotation velocity Ω. On increasing Ω beyond a threshold value, the gain in the magnetic-field energy does not compensate for the loss in the gradient energy from bending $\hat{\mathbf{n}}$ parallel to $\hat{\mathbf{z}}$ at the cylinder axis. To underline the differences between the symmetric and modified flare-out textures, their distributions of $\sin^2\beta$ are presented in Fig. 5. This reflection-symmetric texture has so far not been discovered in measurements, since no systematic studies of the axial-field textures with a SMV have been carried out as a function of Ω.[14]

Since $\sin^2\beta(\mathbf{r})$ is proportional to the local NMR frequency shift, Fig. 5 indicates that the NMR line shapes for the two textures differ markedly from each other. In the case of the reflection-symmetric texture, $\sin^2\beta\gtrsim 0.6$ everywhere and virtually no absorption occurs at low frequencies close to ω_0. Therefore, compared to the flare-out state without the soli-

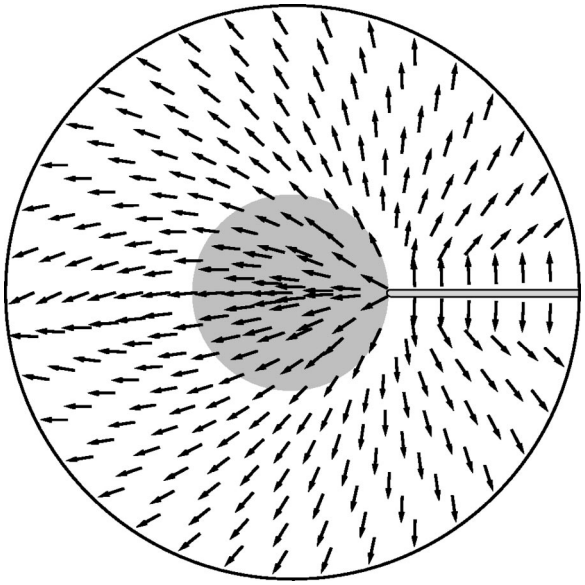

FIG. 4. Calculated equilibrium reflection-symmetric $\hat{\mathbf{n}}$ texture in the presence of a soliton. All external parameters are the same as in Fig. 2, except for $\Omega=2.5$ rad/s.

ton, the NMR signal has a qualitatively different form, which should be readily observable in experiments. A typical line shape for the reflection-symmetric texture, along with the corresponding flare-out texture, is shown in Fig. 6.

Properties of SMV textures. We have compared the energies of both SMV textures as a function of the reduced temperature T/T_c and the rotation velocity Ω. Depending on which has the lowest energy, we have drawn a ''phase diagram'' for the two textures in Fig. 7. The critical angular velocities of the transition are well within the reach of measurements in a rotating cryostat. Apart from the soliton length l, which changes with Ω, the crucial parameter in determining which one of the two textures has the lowest energy in the calculations is the magnetic coherence length ξ_H, which describes the rigidity of $\hat{\mathbf{n}}$. Roughly speaking, a long ξ_H implies more rigidity and prefers the reflection-symmetric texture, which has lower gradient energy. This also explains why it was not observed in Ref. 4, because the measurements were performed very close to T_c, where ξ_H is small. On the other hand, experiments in low magnetic fields and at low temperatures should be favorable to the new texture.

Connection to experiment. Because of metastabilities, measurements of the SMV have to be carefully prepared. They are generally performed at constant pressure, using the following procedure. The first step is to accelerate ^{3}He-A to some high rotation, from where it is slowly decelerated to $\Omega_V+\Omega_{AB}^c$, such that vortex lines are observed to annihilate. This secures the equilibrium number of doubly quantized continuous vortices in the A phase. The next step is to cool slowly through the $A\rightarrow B$ transition at its thermodynamic equilibrium temperature at constant rotation $\Omega_V+\Omega_{AB}^c$. If the $A\rightarrow B$ transition occurs sufficiently slowly, then N_V singly quantized B-phase vortices will be created, corresponding to the equilibrium number at Ω_V and including possibly

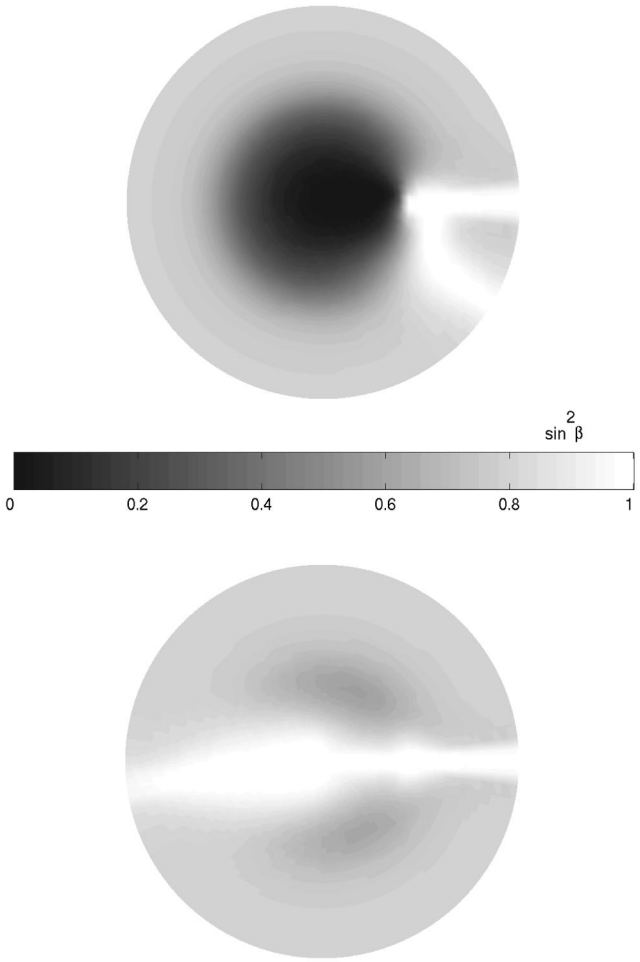

FIG. 5. Distributions of $\sin^2\beta$ in the cylinder with a SMV: (top) modified flare-out texture of Fig. 2 and (bottom) reflection-symmetric texture of Fig. 4. The dark regions ($\sin^2\beta\sim 0$) contribute to NMR absorption at low frequencies close to ω_0, whereas the highest frequencies in the spectrum correspond to the white regions ($\sin^2\beta=1$).

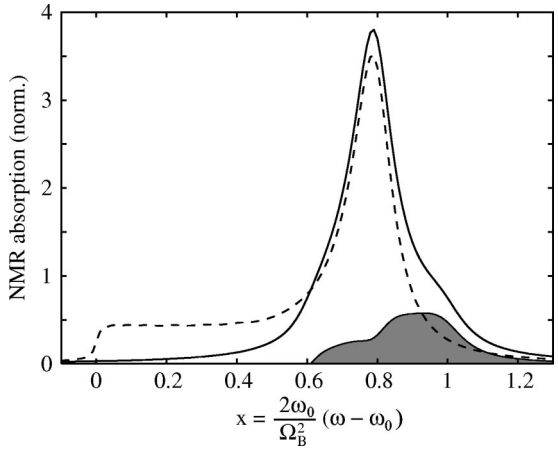

FIG. 6. NMR absorption spectra for the reflection-symmetric texture of Fig. 4 (solid line) and the flare-out texture (dashed line) with the same external parameters. The shaded area is their positive difference. The line broadening parameters are those of Fig. 3.

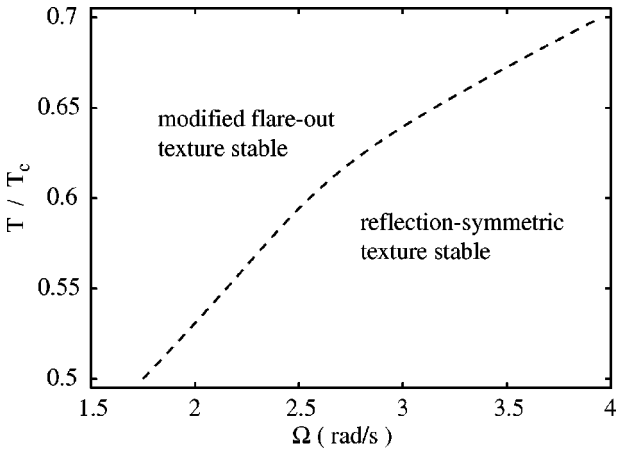

FIG. 7. Stability regions of the modified flare-out and reflection-symmetric textures, calculated with $R=2.9$ mm, $p=29.3$ bars, $H=35.4$ mT, and $N_V=320$ vortex lines.

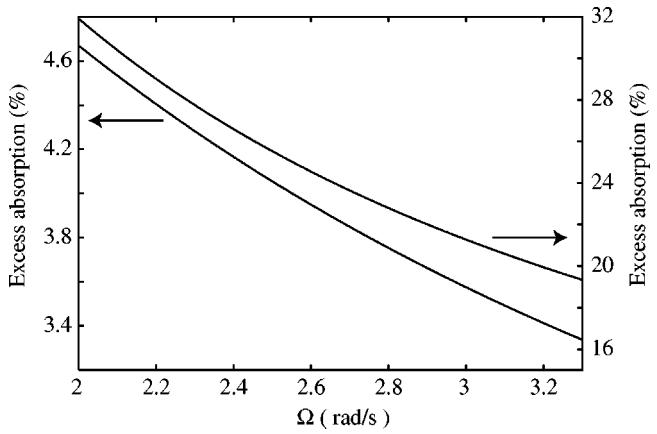

FIG. 8. The integrated *extra* absorption, as defined in Figs. 3 and 6, divided by the integrated *total* absorption, plotted as a function of the rotation velocity, for $R=2.9$ mm, $p=29.3$ bars, $H=20$ mT, and $N_V=320$ vortex lines. The additional line broadening parameters are the same as in Fig. 3. The curve on the left corresponds to the modified flare-out texture at $T=0.8\,T_c$ and the one on the right to the reflection-symmetric texture at $T=0.5\,T_c$ (note the five times larger shifted absorption on the right). Within this Ω range the calculated excess absorptions agree with the following approximate Ω dependences: (1) modified flare-out texture $\propto(1-\sqrt{\Omega_V/\Omega})/\Omega$ and (2) reflection-symmetric texture $\propto 1/\Omega$.

one SMV in the configuration of Fig. 1.[15] This state can then be examined in the B-phase temperature region at rotation velocities which exceed the original value. The second possibility for creating the SMV is to irradiate ^{3}He-B with thermal neutrons, starting with a state in vortex-free rotation above some threshold value of counterflow velocity, as described in Ref. 4.

The rotation velocity of a state with a SMV can be increased to higher values $\Omega>\Omega_V$, since the number of vortex lines can generally be maintained constant at N_V over a large Ω interval, owing to a much higher critical velocity of vortex formation in the B phase.[5] Increasing Ω compresses the existing vortex lines into a cluster with a radius $R_V=R\sqrt{\Omega_V/\Omega}$. Whether or not a SMV is present in this cluster can be deduced by slowing down rotation to Ω_V (which causes the cluster to expand to the wall and the SMV and its soliton tail to annihilate), accelerating back to Ω, and comparing the NMR line shapes before and after this procedure. Here the excess absorption at high NMR frequency shifts (the shaded area in Fig. 3) becomes the crucial quantity in identifying the presence of a SMV. This signal has been extracted from measured NMR spectra on flare-out textures which have been accumulated after a slow $A\rightarrow B$ transition[2] or after neutron irradiation.[4]

To learn more about the properties of the frequency-shifted excess absorption, we have calculated it (relative to the total area under the absorption curve) as a function of Ω. When Ω is increased, the soliton grows in length as $l\approx R(1-\sqrt{\Omega_V/\Omega})$,[1] and one would expect this to increase the shifted absorption. Interestingly, in the calculations the shifted absorption was found to decrease with increasing Ω in both textures (Fig. 8). The reason for this is the simultaneous decrease in the transverse dimension $\sim\xi_H(v_D/v)$ of the region where $\hat{\mathbf{n}}$ differs from the minimum of the counterflow energy. In the case of the reflection-symmetric texture the latter effect is more important, since its distribution of $\hat{\mathbf{n}}$ orientations depends only weakly on the length of the soliton sheet (see Fig. 5).

Conclusion. The experimental NMR signatures have been calculated which identify the presence of the B-phase SMV in axial-magnetic-field order-parameter textures. Two different textures have been found to be stable with the SMV: (a) a distorted flare-out texture at short magnetic textural lengths ξ_H (which corresponds to low rotation and high temperature) and (b) a reflection-symmetric texture at large magnetic lengths.

We thank Erkki Thuneberg for useful discussions.

[1] Y. Kondo, J.S. Korhonen, M. Krusius, V.V. Dmitriev, E.V. Thuneberg, and G.E. Volovik, Phys. Rev. Lett. **68**, 3331 (1992).
[2] J.S. Korhonen, Y. Kondo, M. Krusius, E.V. Thuneberg, and G.E. Volovik, Phys. Rev. B **47**, 8868 (1993).
[3] E.V. Thuneberg, Europhys. Lett. **3**, 711 (1987).
[4] V.B. Eltsov, T.W.B. Kibble, M. Krusius, V.M.H. Ruutu, and G.E. Volovik, Phys. Rev. Lett. **85**, 4739 (2000).
[5] V.M.H. Ruutu, Ü. Parts, J.H. Koivuniemi, N.B. Kopnin, and M. Krusius, J. Low Temp. Phys. **107**, 93 (1997).
[6] G.E. Volovik and V.P. Mineev, Zh. Éksp. Teor. Fiz. **72**, 2256 (1977) [Sov. Phys. JETP **45**, 1186 (1977)].
[7] K. Maki and P. Kumar, Phys. Rev. B **14**, 118 (1976).
[8] H. Smith, W.F. Brinkman, and S. Engelsberg, Phys. Rev. B **15**, 199 (1977).
[9] D.D. Osheroff, Physica B **90**, 20 (1977); D.D. Osheroff, W. van Roosbroeck, H. Smith, and W.F. Brinkman, Phys. Rev. Lett. **38**,

134 (1977).
[10] P.J. Hakonen, M. Krusius, M.M. Salomaa, R.H. Salmelin, J.T. Simola, A.D. Gongadze, G.E. Vachnadze, and G.A. Kharadze, J. Low Temp. Phys. **76**, 225 (1989).
[11] J. Kopu, R. Schanen, R. Blaauwgeers, V.B. Eltsov, M. Krusius, J.J. Ruohio, and E.V. Thuneberg, J. Low Temp. Phys. **120**, 213 (2000).
[12] E.V. Thuneberg, J. Low Temp. Phys. **122**, 657 (2001).
[13] V.M. Ruutu, J.J. Ruohio, M. Krusius, B. Plaçais, and E.B. Sonin, Physica B **255**, 27 (1998).
[14] As a function of Ω, measurements exist in a coherently precessing resonance mode called the ''homogenously precessing domain,'' where the dominant part of the absorption is caused by the soliton tail (Ref. 2). This signal grows with Ω as the length of the soliton sheet: $l/R \approx 1-\sqrt{\Omega_V/\Omega}$.
[15] $\Omega_{AB}^{c} \approx 0.25$ rad/s is the critical velocity required for the doubly quantized *A*-phase circulation to penetrate through the slowly advancing *AB* interface into the *B* phase. See M. Krusius, E.V. Thuneberg, and Ü. Parts, Physica B **197**, 376 (1994).